ORIGINAL UNEDITED MANUSCRIPT

Eu^{3+}-Doped Sr_2LaF_7 Nanopowders as Efficient Red and Deep-Red Emitters for Advanced Horticultural Lighting

Ljubica Đačanin Far[1,*], Jovana Periša[1], Zoran Ristić[1], Anatolijs Šarakovskis[2], Vladimir Pankratov[2], Abdullah Alodhayb[3], Lukasz Marciniak[4], Sanja Kuzman[1], Miroslav D. Dramićanin[1], Bojana Milićević[1]

[1]Centre of Excellence for Photoconversion, Vinča Institute of Nuclear Sciences-National Institute of the Republic of Serbia, University of Belgrade, P.O. Box 522, 11001 Belgrade, Serbia

[2]Laboratory of Spectroscopy, Institute of Solid State Physics, University of Latvia, 8 Kengaraga Street, Riga, Latvia

[3]Research Chair for Tribology, Surface, and Interface Sciences, Department of Physics and Astronomy, College of Science, P.O. BOX 2455, King Saud University, Riyadh, 11451, Saudi Arabia

[4]Institute of Low Temperature and Structure Research, Polish Academy of Sciences, Okolna 2, 50-422 Wroclaw, Poland

Synopsis: Our study presents Eu^{3+}-activated Sr_2LaF_7 nanophosphors with efficient red and deep-red emission, 555% enhanced intensity, and outstanding thermal stability – ideal for next-generation plant growth LEDs.

* ljubica.far@vin.bg.ac.rs
telephone +381113408607
fax +381113408307

© The Author(s) 2026. Published by Oxford University Press on behalf of the Physical Society of Japan. This is an Open Access article distributed under the terms of the Creative Commons Attribution License (https://creativecommons.org/licenses/by/4.0/), which permits unrestricted reuse, distribution, and reproduction in any medium, provided the original work is properly cited.

Downloaded from https://academic.oup.com/ptep/advance-article/doi/10.1093/ptep/ptag026/8472646 by guest on 12 February 2026

ORIGINAL UNEDITED MANUSCRIPT

Abstract

Phosphors applied in agricultural light-emitting diodes (LEDs) for plant growth are designed to convert electrical energy into light within the Photosynthetically Active Radiation (PAR) range, covering wavelengths from 400 to 700 nm. For that purpose, a series of $Sr_2La_{1-x}Eu_xF_7$ (x = 0, 0.05, 0.1, 0.15, 0.2, 0.4, 0.5, 0.6, 0.8) luminescent nanopowders were prepared. Transmission electron microscopy shows nanoparticles of ~33 nm size. The Sr_2LaF_7 sample band gap of 8.8 eV was determined using the reflected electron energy loss spectroscopy method. Photoluminescence measurements show highly efficient red and deep-red emission, with the optimal concentration of 50 mol% of Eu^{3+}, that exhibits a remarkable 555% emission enhancement compared to 5 mol% of Eu^{3+}. The most prominent emission peaks are around 600 nm (orange/red) and 700 nm (deep-red). The observed lifetimes are long, they gradually decrease with the Eu concentration increase, from 14.9 ms for x = 0.05 to 8.3 ms for x = 0.8. Temperature-dependent luminescence spectra to 200°C indicate that the optimal sample exhibits outstanding thermal stability, with emission intensity retaining 97% of its room-temperature value. The quantum efficiency of the optimized sample is 52.73%. The high emission efficiency, wide band gap, good thermal stability and unusual dominant 700 nm deep-red emission make these samples promising nanophosphors for LED-based indoor plant growth.

Keywords: Phosphors; Eu^{3+}; Sr_2LaF_7; deep red emission

Downloaded from https://academic.oup.com/ptep/advance-article/doi/10.1093/ptep/ptag026/8472646 by guest on 12 February 2026

ORIGINAL UNEDITED MANUSCRIPT

1. Introduction

Phosphor materials absorb energy and subsequently re-emit it through the process of luminescence as visible light or in other spectral regions such as ultraviolet or infrared. Lanthanide-based phosphors, renowned for their distinctive physical and chemical properties and wide spectral versatility, are vital components in optoelectronics, lighting, and display technologies. To ensure optimal performance, these phosphors require host matrices that are non-hygroscopic to maintain stability in air and aqueous environments, exhibit low phonon frequencies to minimize non-radiative energy losses, and possess wide band gaps that facilitate efficient dopant transitions while reducing self-absorption effects. Over the past two decades, fluoride compounds have emerged as great candidates for phosphor hosts because of their low phonon energies (300-500 cm^{-1}), high optical transmittance and outstanding chemical stability, which is favorable for enhancing radiative transitions and improving quantum efficiency of phosphors [1,2]. By far, the most widely investigated fluoride hosts belong to the family of alkaline-lanthanide-tetrafluorides − $ALnF_4$ (A=Na, K, Li; Ln^{3+}=Y, La, Gd, Lu) [3–16]. On the other hand, literature reports on alkali-earth-lanthanide based fluorides − M_2LnF_7 (M=Ca, Sr, Ba; Ln^{3+}=Y, La, Gd, Lu) – are scarce and mostly limited to up-conversion phenomenon and related applications of photothermal therapy, anticounterfeiting and bio imaging [17–21]. Only a limited number of published studies propose using phosphors from this family of compounds for light-emitting diode (LED) applications [22–26]. Sr_2LaF_7 has been mostly utilized as a matrix for up-converting ions and applications in photocatalysis [27], optical thermometry [28], fingerprint detection [29], fluorescent labels in near-IR range [30]. To the best of our knowledge, there is only one reported study on $Sr_2LaF_7:Eu^{3+}$,

Downloaded from https://academic.oup.com/ptep/advance-article/doi/10.1093/ptep/ptag026/8472646 by guest on 12 February 2026

ORIGINAL UNEDITED MANUSCRIPT

with doping content up to 30 mol%, obtained by co-precipitation. This powder exhibits red emission with concentration quenching at 20 mol% of Eu^{3+} and lifetimes in ~(4-8) ms range [31]. In modern agriculture, efficient LED lighting is extensively studied for optimizing indoor plant growth. The aim is to maximize electrical energy conversion into Photosynthetically Active Radiation (PAR, 400–700 nm), the spectral part that promotes photosynthesis in plants. Furthermore, recent research also highlights the benefits of deep-red light (700–750 nm), which can elevate photochemical efficiency [32] and improve crop flavor by reducing bitterness in leafy greens like lettuce and spinach. Thus, LED systems combining PAR-aligned and deep-red wavelengths are key to advancing sustainable indoor-based crop production.

In this research, we synthesized Sr_2LaF_7 powders with different contents of Eu^{3+} ions (up to 80 mol%), using a hydrothermal procedure, and proved it has bright red and deep-red emission with long lifetimes of up to ~15 ms. Incorporation of the most optimal nanophosphor onto a 395 nm LED chip showed intense emission indicating great potential for horticulture LED systems.

2. Experimental

The set of Sr_2LaF_7 nanophosphors doped with various concentrations of Eu^{3+} ions (0, 5, 10, 15, 20, 40, 50, 60, and 80 mol%) was synthesized using the hydrothermal procedure. The starting precursors were strontium nitrate ($Sr(NO_3)_2$, Thermo Scientific, 99% min), lanthanum (III) nitrate hexahydrate ($La(NO_3)_3{\cdot}6H_2O$, Alfa Aesar, 99.9%), europium (III) nitrate hexahydrate ($Eu(NO_3)_3{\cdot}6H_2O$, Alfa Aesar, 99.9%), disodium ethylendiaminetetraacetate dihydrate (EDTA-2Na, $C_{10}H_{14}N_2O_8Na_2{\cdot}2H_2O$, Kemika, 99%) and ammonium fluoride (NH_4F, Alfa Aesar, 98%). The

Downloaded from https://academic.oup.com/ptep/advance-article/doi/10.1093/ptep/ptag026/8472646 by guest on 12 February 2026

ORIGINAL UNEDITED MANUSCRIPT

detailed synthesis description and the procedure scheme were given in [26]. In short, precursors were dissolved in de-ionized water and mixed, afterwards the pH was regulated at about 6 using 25 % ammonium hydroxide solution. A hydrothermal reaction took place in a 100-mL Teflon-lined autoclave at 180°C for 20 hours. After cooling, the precipitates were collected by centrifugation, washed twice with deionized water, and once with a 1:1 ethanol-water solution. Finally, the samples were dried in air at 70°C for 4 hours. The exact amounts of precursors needed for preparation of each sample are given in **Table *1***. Although the doping content of Eu^{3+} reaches 80 mol%, the phosphor host is designated as Sr_2LaF_7 (abbreviated name SLF) for the sake of clarity.

Table 1. Precursor quantities required for the synthesis of 0.0025 mol of $Sr_2La_{1-x}Eu_xF_7$ (x = 0, 0.05, 0.1, 0.15, 0.2, 0.4, 0.5, 0.6, 0.8).

Molecular formula	x **[mol% Eu^{3+}]**	**Abbreviated name**	**Precursor mass [g]**				
			$Sr(NO_3)_2$	$La(NO_3)_3 \cdot 6H_2O$	$Eu(NO_3)_3 \cdot 6H_2O$	NH_4F	EDTA-2Na
Sr_2LaF_7	0	SLF		1.0825	-		
$Sr_2La_{0.95}Eu_{0.05}F_7$	5	SLF_5Eu		1.0284	0.0558		
$Sr_2La_{0.9}Eu_{0.1}F_7$	10	SLF_10Eu		0.9743	0.1115		
$Sr_2La_{0.85}Eu_{0.15}F_7$	15	SLF_15Eu		0.9201	0.1673		
$Sr_2La_{0.8}Eu_{0.2}F_7$	20	SLF_20Eu	1.0582	0.8860	0.2230	1.1111	0.9306
$Sr_2La_{0.6}Eu_{0.4}F_7$	40	SLF_40Eu		0.6495	0.4461		
$Sr_2La_{0.5}Eu_{0.5}F_7$	50	SLF_50Eu		0.5413	0.5576		
$Sr_2La_{0.4}Eu_{0.6}F_7$	60	SLF_60Eu		0.4330	0.6691		
$Sr_2La_{0.2}Eu_{0.8}F_7$	80	SLF_80Eu		0.2165	0.8921		

Downloaded from https://academic.oup.com/ptep/advance-article/doi/10.1093/ptep/ptag026/8472646 by guest on 12 February 2026

ORIGINAL UNEDITED MANUSCRIPT

The X-ray diffraction analysis was conducted using a Rigaku SmartLab system with Cu Kα radiation at 30 mA and 40 kV, confirming the phase purity and crystallinity of the samples. Diffraction data were collected in the 2θ range of 10° to 90° with a step size of 0.02° and a counting time of 1°/min, while the structural analysis was performed using the integrated PDXL2 package software. A three-dimensional scheme of crystal structure was built via Diamond 4.6.8 software.

The transmission electron microscope JEOL JEM1011 was used to examine nanopowders microstructure, operating at an accelerating voltage of 100 kV. The average particle size was determined based on size measurement of more than 130 particles, with the help of ImageJ software.

The bandgap of non-doped Sr_2LaF_7 in the pellet form was evaluated by reflected electron energy loss spectroscopy (REELS) measurement. It was carried out using a Thermo Fisher ESCALAB Xi+ instrument, using the electron source energy of 1000 eV, detector pass energy of 10 eV and a step size of 0.02 eV.

Photoluminescent emission and excitation spectra were recorded at room temperature using a Fluorolog-3 Model FL3-221 spectrofluorometer system (Horiba JobinYvon). In a steady-state measurement regime the system was equipped with a 450 W Xenon lamp and TBX detector, while a xenon–mercury pulsed lamp was utilized for emission decay measurements. Excitation spectra were recorded at the fixed emission wavelength of 591 nm and emission spectra were observed upon a 393 nm excitation. The luminescence quantum efficiency was measured using an FLS1000 Fluorescence Spectrometer (Edinburgh Instruments), equipped with a 450 W xenon lamp and an R928 photomultiplier tube (Hamamatsu), coupled with an integrating sphere. The temperature stability of the photoluminescent emission was evaluated over the temperature range of 25–200°C using an OceanOptics spectrofluorometric system with excitation at 365 nm (OceanOptics LED,

Downloaded from https://academic.oup.com/ptep/advance-article/doi/10.1093/ptep/ptag026/8472646 by guest on 12 February 2026

ORIGINAL UNEDITED MANUSCRIPT

L365A), combined with a MicroOptik heating stage. A 395 nm LED chip, delivering 100 mW of optical power, was used to excite a mixture of luminescent powder and a transparent high-temperature inorganic binder (Cerambind 643-2 from Aremco). The emission spectrum of the as-prepared LED device was recorded using the OceanOptics spectrofluorometric system.

3. Results and discussion

3.1. Structure, morphology and band gap analysis

The XRD patterns of the synthesized SLF_xEu (x = 0, 5, 10, 15, 20, 40, 50, 60, 80 mol%) nanopowders exhibit characteristic peaks that coincide well with the ICDD 01-083-3680 data, as shown in **Fig. *1***(a). All the samples belong to the cubic $Fm\bar{3}m$ symmetry space group [31,33], demonstrating that continuous exchange of La^{3+} with Eu^{3+} does not transform the structural type of the compound. This justifies the designation of Sr_2LaF_7 compound as the phosphor host. The schematic view of this structural type is displayed in **Fig. *1***(b), where Sr^{2+} and La^{3+} cations both occupy octahedral Wyckoff sites 4a with m-3m symmetry, while F^- ions reside in tetrahedrally-coordinated Wyckoff sites 8c with −43m symmetry. The ionic radius of doping Eu^{3+} ion is slightly smaller than the radius of the host's La^{3+} ion (La^{3+}_{VIII} = 1.160Å, Eu^{3+}_{VIII} = 1.066Å) [34], and we systematically decreased the La^{3+} content with increasing Eu^{3+} concentration during the synthesis (refer to **Table *1***). Therefore, it is presumable that Eu^{3+} ions exchange La^{3+} ions when incorporating into Sr_2LaF_7 matrix. This assumption is supported by the shifting of diffraction peaks to higher Bragg angles, observable in **Fig. *1***(c). As well as this, the calculated unit cell parameters, presented in **Table *2***, exhibit a decreasing trend with the Eu^{3+} content increase, demonstrating successful doping. The crystallite size calculated from XRD data is around 20 nm for all samples.

Downloaded from https://academic.oup.com/ptep/advance-article/doi/10.1093/ptep/ptag026/8472646 by guest on 12 February 2026

ORIGINAL UNEDITED MANUSCRIPT

Transmission electron micrographs of the representative SLF_50Eu powder, taken with different magnifications, are displayed in **Fig. *1***(d). The microstructure reveals porous, loosely packed agglomerates consisting of nanoparticles with quasi-spherical shapes, a morphology characteristic of fluoride-based nanophosphors obtained through wet-chemical synthesis methods [35]. The particle size histogram fitted with a log-normal distribution, based on more than 130 measured particles, is presented in **Fig. *1***(e)). The particles exhibit a size distribution in 20-80 nm range, with the average particle size estimated to be 33±2 nm. Considering the crystallite size from **Table *2***, we can say that each particle is composed of a few crystallites.

The reflected electron energy loss (REELS) spectrum of the non-doped SLF nanopowder is shown in **Fig. *1***(f). By plotting the electron energy loss spectrum and identifying the onset of inelastic scattering – where intensity begins to rise from the zero-loss peak – the electronic band gap is extracted. In this analysis, that onset corresponds to an energy of 8.8 eV. In the present approach, the background intensity was not explicitly subtracted; instead, the signal onset was estimated from the visible rise above the background slope. Since the tail of the zero-loss peak and the scattering background affect the pre-edge region, this procedure inherently introduces some uncertainty in the determination of the band gap value. Based on repeated measurements and the possible variation in the fitted onset position, we estimated that the uncertainty associated with this method does not exceed 0.2 eV. Large bang gap is favorable for phosphor materials in terms of preventing non-radiative losses, supporting efficient dopant emission and improving thermal and chemical stability.

Downloaded from https://academic.oup.com/ptep/advance-article/doi/10.1093/ptep/ptag026/8472646 by guest on 12 February 2026

ORIGINAL UNEDITED MANUSCRIPT

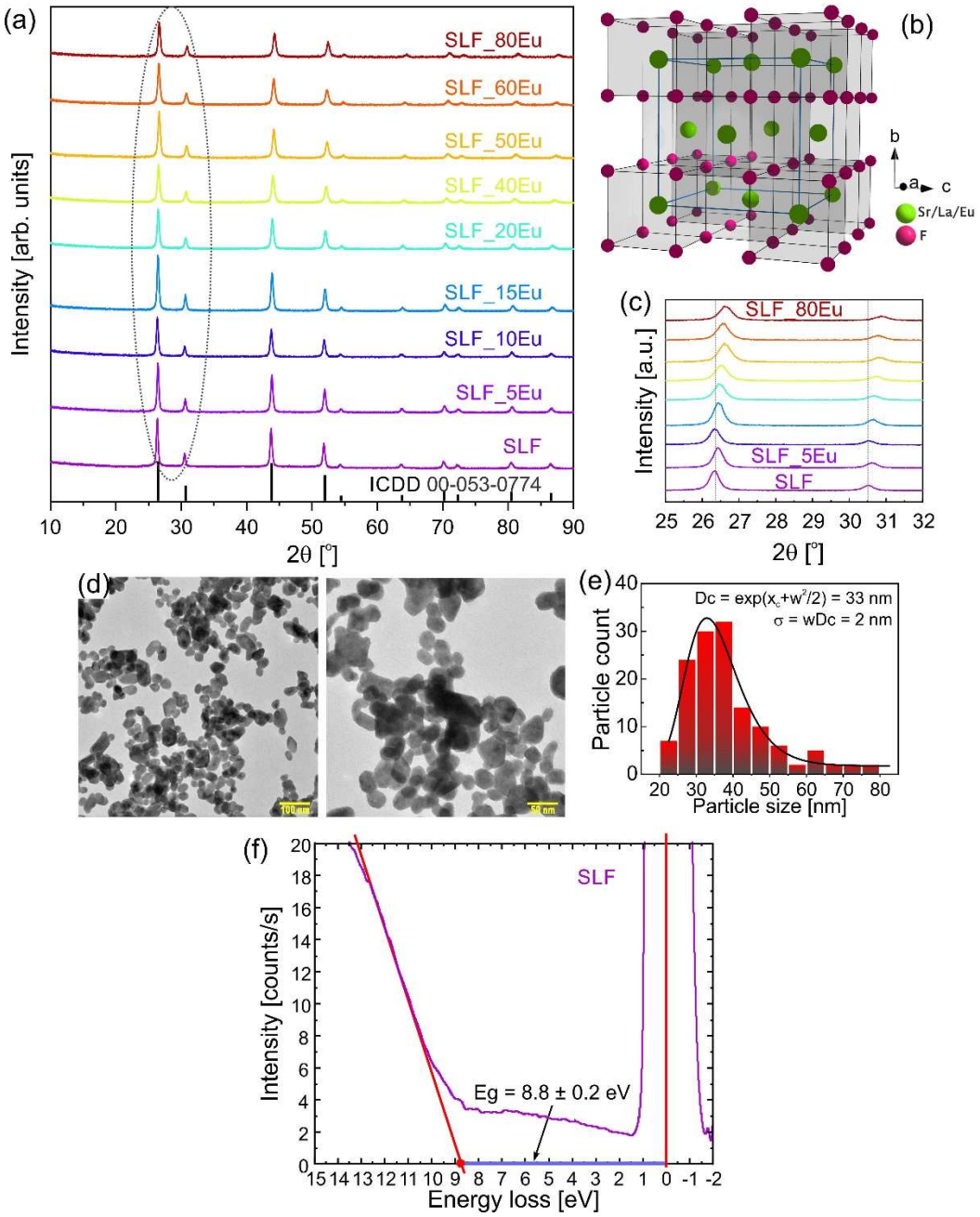

Fig. 1 (a) The XRD patterns of the Sr_2LaF_7 nanophosphors doped with various concentrations of Eu^{3+} ions (5, 10, 15, 20, 40, 50, 60, and 80 mol%), dotted line marking the diffraction peaks from (1 1 1) and (2 0 0) planes; (b) three-dimensional schematic presentation of the cubic Sr_2LaF_7 structure; (c) diffraction data in the *2θ* range of (25-32)°, noting the Bragg angle shift of the (1 1 1) and (2 0 0) peaks; (d) TEM images of the representative SLF_50Eu nanophosphor under different magnifications; (e) particle size distribution

Downloaded from https://academic.oup.com/ptep/advance-article/doi/10.1093/ptep/ptag026/8472646 by guest on 12 February 2026

fitted with lognormal peak function and formulas used for particle size calculation; (f) reflected electron energy loss spectrum of the SLF nanopowder. The blue line represents the band gap energy.

Table 2 Structural parameters of the SLF_*x*Eu (*x* = 0, 5, 10, 15, 20, 40, 50, 60, 80 mol%) nanophosphors.

x **[mol%]**	**0**	**5**	**10**	**15**	**20**	**40**	**50**	**60**	**80**
a=b=c (Å)	5.8401(15)	5.8369(3)	5.8416(6)	5.8355(6)	5.8313(7)	5.8166(5)	5.8048(6)	5.7983(10)	5.7792(13)
CS (nm)	23.1(1)	23.9(7)	22.0(8)	24.8(3)	20.0(3)	21.9(2)	16.6(1)	21.7(4)	22.4(4)
Strain	0.156(3)	0.209(9)	0.205(13)	0.260(3)	0.210(2)	0.360(3)	0.26 (3)	0.390 (3)	0.420 (3)
Rwp	10.08	9.74	10.52	9.21	9.42	8.82	9.04%	7.56%	8.19%
Rp	7.76	7.51	8.19	7.21	7.34	6.98	7.29%	6.07%	6.41%
Re	9.37	9.20	9.54	8.52	8.88	8.27	7.57%	7.45%	7.13%
GOF	1.0750	1.0579	1.1015	1.0809	1.0603	1.0661	1.1939	1.0146	1.1493

R_{wp}—the weighted profile factor; R_p—the profile factor; R_e—the expected weighted profile factor; GOF—the goodness of fit.

3.2. Photoluminescence

The photoluminescence excitation spectrum of the SLF_5Eu sample, recorded by monitoring emission at 591 nm, is presented in **Fig. *2***(a). It exhibits the trivalent europium intra-*4f* electronic transitions, that are noted in **Fig. *2***(a) according to literature [31].

Fig. *2*(b) reveals the emission spectra of the SLF_*x*Eu (*x* = 0, 5, 10, 15, 20, 40, 50, 60, 80 mol%) nanopowders, obtained after a 393 nm excitation. In the wavelength region 500-575 nm, the transitions from the higher excited levels of Eu^{3+} are detected (inset in **Fig. *2***(a)). Dejneka *et al.*[36]

ORIGINAL UNEDITED MANUSCRIPT

Downloaded from https://academic.oup.com/ptep/advance-article/doi/10.1093/ptep/ptag026/8472646 by guest on 12 February 2026

ORIGINAL UNEDITED MANUSCRIPT

reported that in fluoride hosts emissions from $^5D_1$, $^5D_2$, and $^5D_3$ levels can be observed, although their intensity is typically more than order of magnitude less intense than the $^5D_0$ emissions at room temperature. Our results are consistent with this, showing emissions at 510, 526, 535 and 554 nm, that correspond to $^5D_2 \rightarrow {}^7F_3$, $^5D_1 \rightarrow {}^7F_0$, $^5D_1 \rightarrow {}^7F_1$, and $^5D_1 \rightarrow {}^7F_2$ transitions, respectively. However, their intensity is quenched at higher Eu^{3+} concentrations and become negligible at concentrations above 20 mol%. Apart from the higher energy emissions, the typical Eu^{3+} emission transitions around 591 nm ($^5D_0 \rightarrow {}^7F_1$), 613 nm ($^5D_0 \rightarrow {}^7F_2$), 649 nm ($^5D_0 \rightarrow {}^7F_3$) and 698 nm ($^5D_0 \rightarrow {}^7F_4$ transition) are observed [31,37]. The most intense $^5D_0 \rightarrow {}^7F_1$ transition of a magnetic-dipole nature dominates the spectrum, as can be expected for cubic hosts with the activator ion located in centrosymmetric site. The $^5D_0 \rightarrow {}^7F_2$ transition is a forced electric-dipole transition that is highly sensitive to changes in the local environment surrounding the Eu^{3+} ions. All samples show an unusually intense $^5D_0 \rightarrow {}^7F_4$ emission peak near 700 nm, providing a beneficial spectral component that aligns with the deep-red region of the PAR spectrum [38].

Fig. *2*(c) unveils the emission intensity−Eu^{3+} concentration dependence, from which is evident that the maximal intensity is reached at x = 50 mol%, after which the concentration quenching occurs. The SLF_50Eu sample exhibits a remarkable enhancement in emission intensity, reaching 555% relative to the sample with 5 mol% Eu^{3+}. Even at a high doping level of 80 mol%, the emission remains significantly enhanced, showing an intensity 370% greater than that of the lowest-doped sample.

As Dexter and Schulman theory predicts, concentration quenching in inorganic phosphors occurs when energy is transferred from one activator ion to another, typically continuing this process until the energy is ultimately lost to a non-radiative sink within the lattice [39]. The mechanism of concentration quenching can be anticipated by determining the critical distance for energy transfer

Downloaded from https://academic.oup.com/ptep/advance-article/doi/10.1093/ptep/ptag026/8472646 by guest on 12 February 2026

ORIGINAL UNEDITED MANUSCRIPT

between ions, denoted as R_C. The average interaction distance between ions can be approximately calculated using the following equation by Blasse [40]:

$$R_C \approx \left(\frac{6V}{\pi N x_C}\right)^{1/3}. \quad (1)$$

In this expression V [Å^3] represents unit cell volume, N stands for the number of lattice sites per unit cell that can be occupied by activator ions, while x_C is the critical concentration of activator ions, after which the quenching occurs. In our case, $x_C = 0.5$, for $Fm\bar{3}m$ fluorite-type structure $N = 4$, and from XRD data we calculated $V = 195.6$ Å^3. If $R_C > 5$ Å, the multipolar interaction determines concentration quenching, otherwise, the exchange interaction is responsible for it [39]. From Equation (1) we calculated $R_C = 5.72$ Å, so we can conclude that in the case of the SLF_xEu sample series the concentration quenching results from the multipolar interaction. The type of multipolar interaction can be analyzed further using the Van-Uitert equation [41]:

$$\frac{I(x)}{x} = K \cdot \left[1 + \beta \cdot x^{\frac{Q}{3}}\right]^{-1}, \quad (2)$$

where x stands for doping concentration, and $x \geq x_C$; $I(x)$ is the emission intensity for the given concentration, while K and β represent constants. In the case of multipolar interactions, the energy transfer probability is proportional to R^{-Q}, where $Q = 6$, 8 or 10, corresponds to dipole–dipole, dipole–quadrupole, and quadrupole–quadrupole interactions, respectively. With the approximation $\beta \cdot x^{\frac{Q}{3}} \gg 1$, and by linearizing the Eq.(2), the following relation is obtained:

Downloaded from https://academic.oup.com/ptep/advance-article/doi/10.1093/ptep/ptag026/8472646 by guest on 12 February 2026

$$\log\left[\frac{I(x)}{x}\right] = logK_1 - \frac{Q}{3}\log x\,, \qquad K_1 = K \cdot \beta^{-1}. \tag{3}$$

The inset in **Fig. *2***(c) displays the function $log(I/x) - \log x$, for $x \geq x_C$. The parameter Q was calculated from the slope of the linear fit. In this case, $Q = 5.4 \pm 0.87$, which is closest to the theoretical value of 6, indicating that dipole-dipole interactions are the dominant mechanism responsible for concentration quenching in the SLF_xEu sample set.

Normalized time decay curves of the SLF_xEu nanopowders are depicted in **Fig. *2***(d). The decay profiles were evaluated by applying a single-exponential fitting to the experimental data, thereby determining the corresponding lifetimes (τ) according to equation:

$$I(t) = I_0 e^{-\frac{t}{\tau}}, \tag{4}$$

where $I(t)$ represents the emission intensity at time t, I_0 is the corresponding emission intensity at time $t = 0$ (ideally, $I_0 = 1$ for normalized intensity), while τ represents the excited state lifetime. All the excited $^5D_0$ state lifetimes are very long and decrease within (14.9-8.3) ms range as the Eu^{3+} content increases (see inset in **Fig. *2***(d)). Compared to previously published research on Eu^{3+}-activated Sr_2LaF_7 nanophosphors [31], our measured lifetime values are approximately twice as high, aligning closely with those observed in similar fluoride-based matrices [26].

The optimized SLF_50Eu sample exhibits a quantum efficiency of 52.73%, indicating efficient radiative emission. This value is regarded as substantial, particularly for Eu^{3+}-doped fluoride hosts [42–44], given that red-emitting Eu^{3+} transitions often experience non-radiative relaxation

ORIGINAL UNEDITED MANUSCRIPT

Downloaded from https://academic.oup.com/ptep/advance-article/doi/10.1093/ptep/ptag026/8472646 by guest on 12 February 2026

pathways. This result highlights the excellent luminescent performance and favorable energy transfer dynamics within the SLF host lattice.

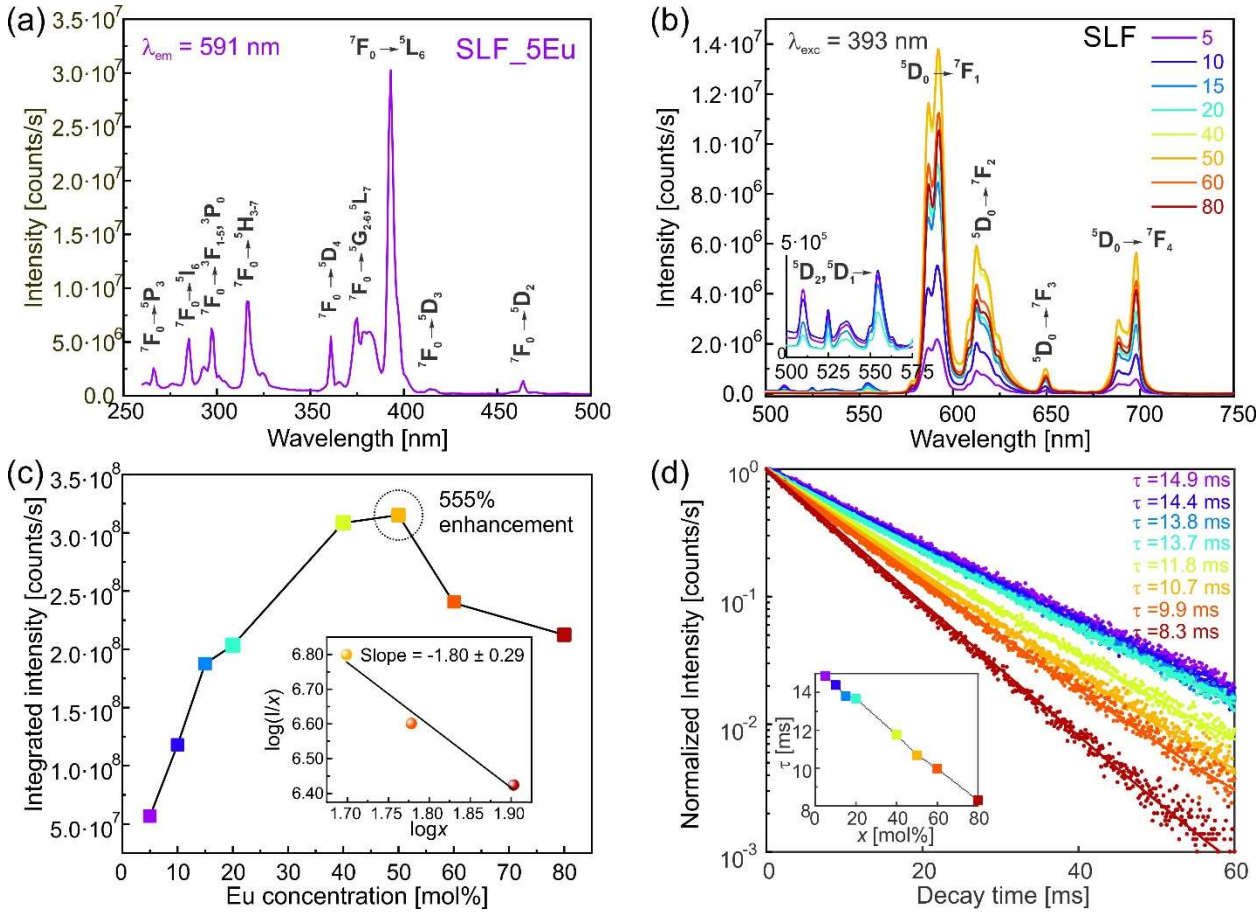

Fig. 2 (a) The excitation spectrum of SLF_5Eu, recorded under a 591 nm emission; (b) the emission spectra of SLF_xEu (x = 0, 5, 10, 15, 20, 40, 50, 60, 80 mol%) nanophosphors. The inset shows 500-575 nm spectral range. (c) The intensity-concentration dependence of the SLF_xEu nanopowders. The inset: $log(I/x)$ vs. $logx$ plot, for $x \geq x_C$. The measurement uncertainty is comparable to, or smaller than the symbol size. (d) The excited state decay curves for different Eu^{3+} concentrations. The inset: lifetime values vs. Eu^{3+} concentration.

ORIGINAL UNEDITED MANUSCRIPT

Downloaded from https://academic.oup.com/ptep/advance-article/doi/10.1093/ptep/ptag026/8472646 by guest on 12 February 2026

ORIGINAL UNEDITED MANUSCRIPT

3.3. CIE coordinates, emission stability and LED fabrication

For horticultural LED applications, selecting the appropriate light color and ensuring the thermal stability of photoluminescence emission are critical requirements.

To evaluate the color characteristics of the synthesized nanophosphors, the CIE chromaticity coordinates were calculated from the emission spectra shown in **Fig. *2***(b). The CIE (Commission Internationale de l'Éclairage) 1931 chromaticity diagram provides a standardized method for representing and describing colors using the (x, y) coordinates, which indicate the chromaticity of a light source independent of its brightness. Additionally, the color purity of the emitted light was evaluated to assess the degree of color saturation, where a higher purity value indicates a more vivid and saturated color. **Table *3*** features the colorimetric parameters of the examined nanopowders, derived from the corresponding emission spectra, while **Fig. *3***(a) illustrates the position in the CIE diagram. The (x, y) chromaticity coordinates of all samples fall within the red region of the diagram, showing a gradual shift from orange-red to deep red as the Eu^{3+} concentration increases. The color purity is exceptional, reaching 100% pure color after x = 20 mol%.

Table 3 Colorimetric parameters of SLF_xEu (x = 5, 10, 15, 20, 40, 50, 60, 80 mol%) nanophosphors

X [mol%]	5	10	15	20	40	50	60	80
x	0.550	0.576	0.594	0.599	0.604	0.607	0.607	0.607
y	0.441	0.419	0.404	0.400	0.395	0.392	0.393	0.392
Color purity[%]	92.44	98.32	98.95	99.67	100	100	100	100

Downloaded from https://academic.oup.com/ptep/advance-article/doi/10.1093/ptep/ptag026/8472646 by guest on 12 February 2026

ORIGINAL UNEDITED MANUSCRIPT

To assess the thermal stability of nanophosphors, steady-state temperature-dependent emission measurements were performed over the range of 25°C to 200°C, in 25°C increments, using the SLF_50Eu sample pressed into a pellet. While some LED manufacturers consider 100°C as the typical maximum operating temperature for LEDs [45,46], literature reports often indicate temperature stability up to 150°C [47,48]. As shown in **Fig. *3***(a), the SLF_50Eu sample exhibits remarkable thermal stability, retaining almost 100% of its room-temperature integrated emission intensity up to 100°C and still maintaining 97% of its initial emission intensity at 200°C. Moreover, the inset in **Fig. *3***(b) demonstrates considerable temporal stability of this nanophosphor.

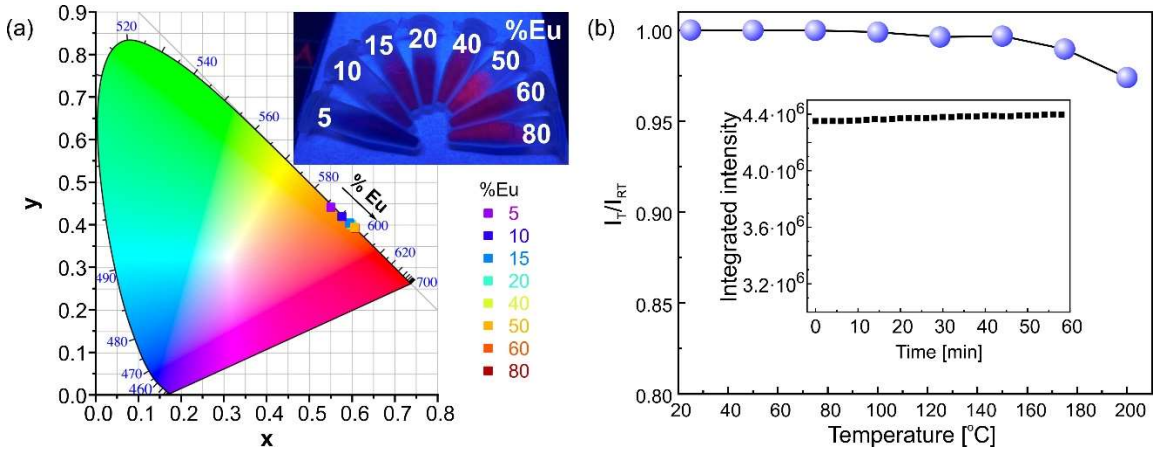

Fig. 3 (a) Position in the CIE color diagram of the SLF_xEu (x = 0, 5, 10, 15, 20, 40, 50, 60, 80 mol%) nanophosphors. The inset: synthesized nanopowders under an UV lamp lighting; (b) Thermal stability of photoluminescence emission of the SLF_50Eu sample. The inset shows temporal stability of the integrated emission intensity.

To evaluate the practical applicability of the phosphors in LED technology, the powder sample with the highest emission intensity, SLF_50Eu, was combined with a ceramic binder and coated

Downloaded from https://academic.oup.com/ptep/advance-article/doi/10.1093/ptep/ptag026/8472646 by guest on 12 February 2026

ORIGINAL UNEDITED MANUSCRIPT

onto a 395 nm near-UV LED chip. As shown in **Fig. *4***(a) , the fabricated LED device emits a strong red light when powered. The corresponding emission spectrum, presented in **Fig. *4***(b) clearly displays the characteristic europium emission transitions in the red and deep-red spectral regions. The dashed line in Fig. 4(b) corresponds to the emission spectrum of the 395 nm chip. The two peaks observed near 400 nm arise from the chip's emission and the Eu^{3+} absorption transition $^7F_0 \rightarrow {}^5L_6$ at 393 nm (see excitation spectrum in **Fig. *2***(a)). The strong overlap between these transitions enables efficient energy absorption by Eu^{3+} ions, producing the characteristic doublet around 400 nm.

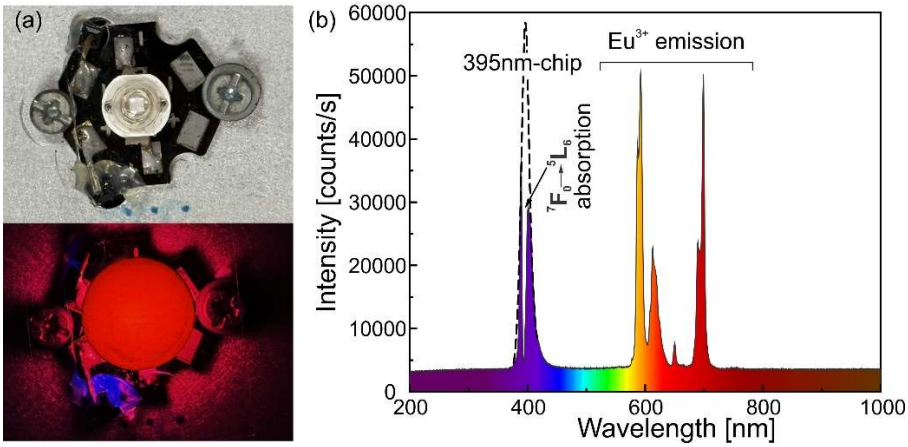

Fig. 4 (a) LED device, fabricated from a SLF_50Eu nanophosphor with a binder on a 395 nm-emitting semiconductor chip, displaying strong red light; (b) the emission spectrum of the as-prepared LED device. The dashed line represents the emission spectrum of a 395 nm chip. The dip at 393 nm corresponds to the $^7F_0 \rightarrow {}^5L_6$ absorption transition of Eu^{3+}.

Downloaded from https://academic.oup.com/ptep/advance-article/doi/10.1093/ptep/ptag026/8472646 by guest on 12 February 2026

ORIGINAL UNEDITED MANUSCRIPT

4. Conclusion

In this research, a series of Sr_2LaF_7 nanoparticles was synthesized via hydrothermal method and doped with various concentrations of Eu^{3+} ions. We conducted a comprehensive analysis of their structural, morphological and photoluminescent properties, and demonstrated:

- The Sr_2LaF_7 host material possesses a wide band gap of 8.8 eV, well-suited for activation with different lanthanide ions.
- The emission spectra upon a 393 nm excitation reveal intense orange/red and deep-red emission of Eu^{3+}.
- The most dominant $^5D_0 \rightarrow {}^7F_1$ transition typical for centrosymmetric environments is accompanied by an unusually intense $^5D_0 \rightarrow {}^7F_4$ transition.
- The emission intensity increases with increasing Eu^{3+} concentration, peaking at x = 50 mol%, beyond which concentration quenching is observed—attributed to a dipole–dipole interaction mechanism.
- The excited-state lifetimes decrease from ~15 ms for x = 5 to ~8 ms for x = 80 mol%.
- The optimized SLF_50Eu sample exhibits a remarkable 555% enhancement in integrated emission intensity compared to the lowest concentration, while even at 80 mol% of Eu^{3+}, the emission remains enhanced by 370%.
- The quantum efficiency of the optimized sample is 52.73%.
- The nanophosphors demonstrate excellent thermal stability, retaining 100% of their room-temperature emission at 100°C and 97% at 200°C.

Downloaded from https://academic.oup.com/ptep/advance-article/doi/10.1093/ptep/ptag026/8472646 by guest on 12 February 2026

ORIGINAL UNEDITED MANUSCRIPT

These findings confirm the potential of $Sr_2LaF_7:Eu^{3+}$ nanophosphors as efficient red-emitting materials for LED-based applications, particularly in indoor plant growth lighting. Future work will focus on evaluating their performance in integrated LED systems for plant growth lighting.

Downloaded from https://academic.oup.com/ptep/advance-article/doi/10.1093/ptep/ptag026/8472646 by guest on 12 February 2026

Acknowledgement

This research was supported by the Science Fund of the Republic of Serbia, #GRANT No 10412, LED technology based on bismuth-sensitized Eu^{3+} luminescence for cost-effective indoor plant growth - LEDTech-GROW (Authors: Lj. Đačanin Far, J. Periša, S. Kuzman, B. Milićević). The authors Lj. Đačanin Far, J. Periša, Z. Ristić, S. Kuzman, M.D. Dramićanin and B. Milićević acknowledge funding from the Ministry of Science, Technological Development, and Innovation of the Republic of Serbia under contract 451-03-136/2025-03/ 200017. Author A. Alodhayb would like to acknowledge the Ongoing Research Funding Program–Research Chairs (ORF-RC-2025-1611), King Saud University, Riyadh, Saudi Arabia.

Conflicts of interest The authors declare there are no conflicts of interest.

Data availability The data supporting the results can be accessed in Zenodo repository at 10.5281/zenodo.17092218, as well as upon request directly to the corresponding author.

Author contributions: CRediT

Lj. Đačanin Far Writing - Original Draft, Data Curation, Visualization, Investigation, Project administration, **J. Periša** Investigation, **Z. Ristić** Investigation, Formal analysis, **A. Šarakovskis** Investigation, **V. Pankratov** Investigation, **L. Marciniak** Investigation, **A. Alodhayb**

Investigation, **S. Kuzman** Investigation, **M.D. Dramićanin** Writing - Review & Editing, Conceptualization, Supervision, Resources **B. Milićević** Writing - Review & Editing, Conceptualization, Supervision, Funding acquisition, Project administration

References

[1] V.B. Pawade, N.R. Pawar, S.J. Dhoble, Upconversion in some fluoride crystal system –A review, Infrared Phys Technol 123 (2022) 104148. https://doi.org/10.1016/j.infrared.2022.104148.

[2] R.K. Sharma, A.-V. Mudring, P. Ghosh, Recent trends in binary and ternary rare-earth fluoride nanophosphors: How structural and physical properties influence optical behavior, J Lumin 189 (2017) 44–63. https://doi.org/10.1016/j.jlumin.2017.03.062.

[3] S. Liu, Y. Chen, S. Wang, Z. Zhou, R. Zhang, X. Cheng, G. Liang, Q. Hu, High-fluoride-induced rapid synthesis and universal modulation of hexagonal phase NaYF4, Opt Mater (Amst) 164 (2025) 116987. https://doi.org/10.1016/j.optmat.2025.116987.

[4] P.P. Fedorov, I.I. Buchinskaya, Sodium fluoride and rare earth trifluorides systems. Review, Kondensirovannye Sredy i Mezhfaznye Granitsy = Condensed Matter and Interphases 26 (2024) 687–705. https://doi.org/10.17308/kcmf.2024.26/12415.

[5] M. Suta, What makes β-$NaYF_4$:Er^{3+},Yb^{3+} such a successful luminescent thermometer?, Nanoscale 17 (2025) 7091–7099. https://doi.org/10.1039/D4NR04392H.

[6] Y. Xiao, Q. Luo, M. Ju, Y. Yeung, Quantitatively Deciphering the Local Structure and Luminescence Spectroscopy of Pr^{3+} -Doped Yttrium Lithium Fluoride, J Phys Chem A 128 (2024) 9107–9113. https://doi.org/10.1021/acs.jpca.4c03698.

[7] M.S. Kumar, S. Bedamati, M. Behera, R. Arun Kumar, M. Ramudu, K. Kumar, P. Wozny, K. Soler-Carracedo, M. Runowski, Efficient multi-functional erbium-doped lithium yttrium fluoride phosphor synthesized by novel microwave-assisted combustion technique for diverse applications, Mater Res Bull 190 (2025) 113484. https://doi.org/10.1016/j.materresbull.2025.113484.

[8] H. Ren, M. Huang, S. Ling, B. Li, S. Lan, Q. Tan, S. Liao, L. Hou, Y. Huang, Electronic defect engineering of double-doped β-KYF4:Eu3+,Bi3+ red phosphors: Negative thermal quenching and applications for high-efficiency white light-emitting diodes, J Solid State Chem 339 (2024) 124939. https://doi.org/10.1016/j.jssc.2024.124939.

[9] M. Sedano, S. Babu, R. Balda, J. Fernández, A. Durán, M.J. Pascual, Spark plasma sintering and optical properties of Tm3+ and Tm3+ /Yb3+ doped NaLaF4 transparent glass-ceramics, J Alloys Compd 948 (2023) 169552. https://doi.org/10.1016/j.jallcom.2023.169552.

ORIGINAL UNEDITED MANUSCRIPT

Downloaded from https://academic.oup.com/ptep/advance-article/doi/10.1093/ptep/ptag026/8472646 by guest on 12 February 2026

ORIGINAL UNEDITED MANUSCRIPT

[10] X. Li, Y. Li, D. Jia, G. Hu, D. Zhang, S. Jin, M. Wang, Luminescence enhancement of NaGdF4:Yb,Er,Li and its improving effect on the photocatalytic degradation of ZnIn2S4, Opt Mater (Amst) 162 (2025) 116812. https://doi.org/10.1016/j.optmat.2025.116812.

[11] X. Wang, R. Wang, Y. Jin, J. Liu, Y. Chu, Y. Tian, J. Ren, L. Liu, J. Zhang, Two-mode upconversion color-tuning of Er:$NaYbF_4$ nanocrystals and their high-efficiency photothermal conversion, J Mater Chem C Mater (2025). https://doi.org/10.1039/D5TC01139F.

[12] E.I. Oleynikova, O.A. Morozov, S.L. Korableva, M.S. Pudovkin, LiGdxY1−xF4 and LiGdF4:Eu3+ Microparticles as Potential Materials for Optical Temperature Sensing, Ceramics 7 (2024) 276–290. https://doi.org/10.3390/ceramics7010018.

[13] S. Zhang, Y. Xie, X. Hu, X. Zheng, P. Huang, X. Wang, H. Zhang, W. Zheng, X. Chen, Time-resolved luminescent biodetection of biotin in infant formula based on lanthanide-doped LiLuF4 nanoparticles, J Lumin 285 (2025) 121312. https://doi.org/10.1016/j.jlumin.2025.121312.

[14] I.S. Deo, M. Gupta, G.V. Prakash, Up- and Downconversion Dual-Mode Excitation Spectral Studies of Rare Earth Doped $KLaF_4$ Nano Emitters for Biophotonic Applications, The Journal of Physical Chemistry C 127 (2023) 24233–24241. https://doi.org/10.1021/acs.jpcc.3c05125.

[15] J. K, G. E, V. V, R. S, T. P, Emission colour tuning in KLnF4:Yb3+,Er3+/Ho3+ phosphor, Journal of Rare Earths 42 (2024) 57–65. https://doi.org/10.1016/j.jre.2023.02.014.

[16] Q. Min, W. Bian, Y. Qi, W. Lu, X. Yu, X. Xu, D. Zhou, J. Qiu, Temperature sensing based on the up-conversion emission of Tm3+ in a single KLuF4 microcrystal, J Alloys Compd 728 (2017) 1037–1042. https://doi.org/10.1016/j.jallcom.2017.09.050.

[17] W. Wang, X. Wei, H. Chen, Y. Pan, Y. Li, Tunable up-conversion in glass–ceramics containing Ba2YF7: Ho3+/Yb3+ nanocrystals via Ce3+ doping, Applied Physics A 128 (2022) 304. https://doi.org/10.1007/s00339-022-05424-0.

[18] C. Shen, H. Cheng, S. Ma, K. Zhang, T. Li, Dual-mode photoluminescence of Ba_2GdF_7: Yb^{3+}, Er^{3+}, Eu^{3+} spheroidal nanoparticles for optical anticounterfeiting, Journal of the American Ceramic Society 108 (2025). https://doi.org/10.1111/jace.20601.

[19] H. Li, Y. Zhao, I. Kolesnikov, S. Xu, L. Chen, G. Bai, Multifunctional rare earth ions-doped Ba2LaF7 nanocrystals for simultaneous temperature sensing and photothermal therapy, J Alloys Compd 931 (2023) 167535. https://doi.org/10.1016/j.jallcom.2022.167535.

[20] Y. Wang, C. Ji, Y. Tan, L. Xiang, J. Hou, Construction of multifunctional lanthanide-based nanoparticles Ba2LuF7: Yb/Er/Ho for in vivo dual-modal tumor imaging, Opt Mater (Amst) 128 (2022) 112369. https://doi.org/10.1016/j.optmat.2022.112369.

[21] K.S. Janbandhu, V.B. Pawade, S.J. Dhoble, Photon upconversion luminescence in Ho3+/Yb3+ doped Sr2YF7 nanophosphors synthesized by wet chemical method, Mater Lett 341 (2023) 134246. https://doi.org/10.1016/j.matlet.2023.134246.

[22] M. Yan, X. Pei, Y. Liu, L. Fan, T. Jiang, Z. Mi, L. Liu, C. Li, H. Lin, S. Li, W. Yang, F. Zeng, Z. Su, Structure and luminescence study of Gd3+ sensitized Sr2YF7: Eu3+: A novel red

Downloaded from https://academic.oup.com/ptep/advance-article/doi/10.1093/ptep/ptag026/8472646 by guest on 12 February 2026

ORIGINAL UNEDITED MANUSCRIPT

luminescent phosphor for high-performance white light diodes and fingerprints, Ceram Int 51 (2025) 19267–19281. https://doi.org/10.1016/j.ceramint.2025.02.103.

[23] M. Yan, Y. Liu, X. Pei, L. Fan, L. Liu, C. Li, H. Lin, S. Li, W. Yang, F. Zeng, Z. Su, A novel Gd3+-doping-induced enhancement of Sr2YF7: Dy3+ phosphor photoluminescence and thermal stability for white light-emitting diodes, J Alloys Compd 1020 (2025) 179509. https://doi.org/10.1016/j.jallcom.2025.179509.

[24] A.C. Yanes, J. del-Castillo, Enhanced red and green emissions in Sr2GdF7-based nano-glass-ceramics through Ce3+ sensitization and energy migration, Opt Mater (Amst) 159 (2025) 116567. https://doi.org/10.1016/j.optmat.2024.116567.

[25] M. Yan, L. Liu, Y. Wang, Y. Liu, X. Pei, L. Fan, H. Lin, S. Li, W. Yang, Z. Su, C. Li, F. Zeng, Energy transfer mechanism and luminescence properties of green phosphors Sr2YF7: Dy3+, Tb3+, J Lumin 269 (2024) 120438. https://doi.org/10.1016/j.jlumin.2024.120438.

[26] B. Milićević, A. Ćirić, Z. Ristić, M. Medić, A.N. Alodhayb, I.R. Evans, Ž. Antić, M.D. Dramićanin, Eu3+- activated Sr2GdF7 colloid and nano-powder for horticulture LED applications, J Alloys Compd 1010 (2025) 177820. https://doi.org/10.1016/j.jallcom.2024.177820.

[27] Y. Li, Y. Zhang, J. Wang, Y. Fan, T. Xiao, Z. Yin, T. Wang, J. Qiu, Z. Song, Enhancement of solar-driven photocatalytic activity of oxygen vacancy-rich Bi/BiOBr/Sr2LaF7:Yb3+,Er3+ composites through synergetic strategy of upconversion function and plasmonic effect, Journal of Environmental Sciences 115 (2022) 76–87. https://doi.org/10.1016/j.jes.2021.05.036.

[28] S. Li, W. Wang, X. Wei, L. Li, Q. Zhang, Y. Li, Y. Pan, Luminescent properties of Sr2LaF7: Yb3+/Er3+ nanocrystals embedded in glass ceramics for optical thermometry, Opt Mater (Amst) 113 (2021) 110840. https://doi.org/10.1016/j.optmat.2021.110840.

[29] K.S. Janbandhu, V.B. Pawade, J.B. Modak, Intense green emitting Ho3+/Yb3+ Co-doped Sr2LaF7 upconversion nanocrystals for latent fingerprint detection, Mater Res Bull 190 (2025) 113536. https://doi.org/10.1016/j.materresbull.2025.113536.

[30] B. Milićević, J. Periša, Z. Ristić, K. Milenković, Ž. Antić, K. Smits, M. Kemere, K. Vitols, A. Sarakovskis, M. Dramićanin, Hydrothermal Synthesis and Properties of Yb3+/Tm3+ Doped Sr2LaF7 Upconversion Nanoparticles, Nanomaterials 13 (2022) 30. https://doi.org/10.3390/nano13010030.

[31] M. Runowski, S. Balabhadra, S. Lis, Nanosized complex fluorides based on Eu3+ doped Sr2LnF7 (Ln=La, Gd), Journal of Rare Earths 32 (2014) 242–247. https://doi.org/10.1016/S1002-0721(14)60058-2.

[32] S. Zhen, B. Bugbee, Far-red photons have equivalent efficiency to traditional photosynthetic photons: Implications for redefining photosynthetically active radiation, Plant Cell Environ 43 (2020) 1259–1272. https://doi.org/10.1111/pce.13730.

[33] Y. Mao, M. Ma, L. Gong, C. Xu, G. Ren, Q. Yang, Controllable synthesis and upconversion emission of ultrasmall near-monodisperse lanthanide-doped Sr2LaF7 nanocrystals, J Alloys Compd 609 (2014) 262–267. https://doi.org/10.1016/j.jallcom.2014.04.168.

Downloaded from https://academic.oup.com/ptep/advance-article/doi/10.1093/ptep/ptag026/8472646 by guest on 12 February 2026

ORIGINAL UNEDITED MANUSCRIPT

[34] R.D. Shannon, Revised effective ionic radii and systematic studies of interatomic distances in halides and chalcogenides, Acta Crystallographica Section A 32 (1976) 751–767. https://doi.org/10.1107/S0567739476001551.

[35] K. Milenković, L. Đačanin Far, S. Kuzman, Ž. Antić, A. Ćirić, M.D. Dramićanin, B. Milićević, Red emission enhancement in $BaYF_5:Eu^{3+}$ phosphor nanoparticles by Bi^{3+} co-doping, Opt Express 32 (2024) 41632. https://doi.org/10.1364/OE.542685.

[36] M. Dejneka, E. Snitzer, R.E. Riman, Blue, green and red fluorescence and energy transfer of Eu3+ in fluoride glasses, J Lumin 65 (1995) 227–245. https://doi.org/10.1016/0022-2313(95)00073-9.

[37] M. Sekulić, T. Dramićanin, A. Ćirić, L. Đačanin Far, M.D. Dramićanin, V. Đorđević, Photoluminescence of the Eu3+-Activated YxLu1−xNbO4 (x = 0, 0.25, 0.5, 0.75, 1) Solid-Solution Phosphors, Crystals (Basel) 12 (2022) 427. https://doi.org/10.3390/cryst12030427.

[38] H. Li, Y. Niu, C. Liu, H. Jiang, J. Li, J. Wu, S. Huang, H. Zhang, J. Zhu, Unraveling the Remarkable Influence of Square Antiprism Geometry on Highly Efficient Far-Red Emission of Eu^{3+} in Borotellurate Phosphors for Versatile Utilizations, Laser Photon Rev 18 (2024). https://doi.org/10.1002/lpor.202400843.

[39] D.L. Dexter, J.H. Schulman, Theory of Concentration Quenching in Inorganic Phosphors, J Chem Phys 22 (1954) 1063–1070. https://doi.org/10.1063/1.1740265.

[40] G. Blasse, Energy transfer in oxidic phosphors, Phys Lett A 28 (1968) 444–445. https://doi.org/10.1016/0375-9601(68)90486-6.

[41] L.G. Van Uitert, Characterization of Energy Transfer Interactions between Rare Earth Ions, J Electrochem Soc 114 (1967) 1048. https://doi.org/10.1149/1.2424184.

[42] M.T. Tran, N. Van Quang, N.T. Huyen, N. Tu, N. Van Du, D.Q. Trung, N.T. Tuan, N.D. Hung, D.X. Viet, D.T. Tung, N.D. Trung Kien, T.T. Hao Tam, P.T. Huy, High quantum efficiency and excellent color purity of red-emitting Eu^{3+} -heavily doped $Gd(BO_2)_3$ -Y_3BO_6 -$GdBO_3$ phosphors for NUV-pumped WLED applications, RSC Adv 13 (2023) 25069–25080. https://doi.org/10.1039/D3RA03955B.

[43] Z.-J. Zhang, W. Yang, Enhanced quantum efficiency and controllable emissions of Eu through incorporation of Mn2+ in β-NaYF4 nanocrystals, Opt Mater (Amst) 92 (2019) 167–173. https://doi.org/10.1016/j.optmat.2019.04.031.

[44] S. Kaur, S. Arora, A.S. Rao, Comparative study of luminescence in alkali-metal-based yttrium fluoride nanophosphor for biophotonic applications, Int J Appl Ceram Technol 21 (2024) 3700–3712. https://doi.org/10.1111/ijac.14805.

[45] https://downloads.cree-led.com/files/fs/XLamp-Discrete-Directional-Feature-Sheet.pdf, (n.d.).

[46] https://ams-osram.com/products/leds/color-leds/osram-chip-led-0402-lb-qh9g, (n.d.).

Downloaded from https://academic.oup.com/ptep/advance-article/doi/10.1093/ptep/ptag026/8472646 by guest on 12 February 2026

[47] Y. Liu, J. Zhang, C. Zhang, J. Xu, G. Liu, J. Jiang, H. Jiang, $Ba_9Lu_2Si_6O_{24}:Ce^{3+}$: An Efficient Green Phosphor with High Thermal and Radiation Stability for Solid-State Lighting, Adv Opt Mater 3 (2015) 1096–1101. https://doi.org/10.1002/adom.201500078.

[48] C. Yang, W. Liu, Q. You, X. Zhao, S. Liu, L. Xue, J. Sun, X. Jiang, Recent Advances in Light-Conversion Phosphors for Plant Growth and Strategies for the Modulation of Photoluminescence Properties, Nanomaterials 13 (2023) 1715. https://doi.org/10.3390/nano13111715.

ORIGINAL UNEDITED MANUSCRIPT

Downloaded from https://academic.oup.com/ptep/advance-article/doi/10.1093/ptep/ptag026/8472646 by guest on 12 February 2026